Nanoscale

Accepted Manuscript

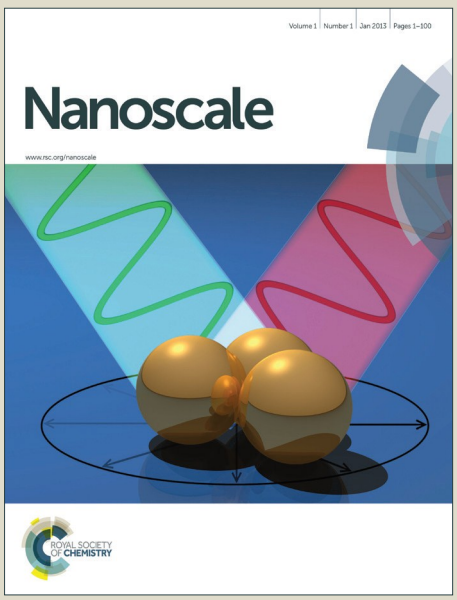

ROYAL SOCIETY OF CHEMISTRY

www.rsc.org/nanoscale

Nanoscale

ARTICLE

Highly cross-linked Cu/a-Si core-shell nanowires for ultra-long cycle life and high rate lithium battery

Received 00th January 20xx,
Accepted 00th January 20xx

DOI: 10.1039/x0xx00000x

www.rsc.org/

Hongxiang Wang,[a] Hucheng Song,[a] Zixia Lin,[a] Xiaofan Jiang, [a] Xiaowei Zhang,[a] Linwei YU,*[a] Jun XU,[a] Lijia Pan,[a] Junzhuan Wang,*[a] Mingbo Zheng,[a] Yi Shi,[a] and Kunji Chen [a]

Seeking long cycle lifetime and high rate performance are still challenging aspects to promote the application of silicon-loaded lithium ion batteries (LIBs), where optimal structural and compositional design are critical to maximize a synergistic effect in composite core-shell nanowire anode structures. We here propose and demonstrate a high quality conformal coating of amorphous Si (a-Si) thin film over a matrix of highly cross-linked CuO nanowires (NW). The conformal a-Si coating can serve as both a high capacity storage medium and a high quality binder that joins crossing CuO NWs into a continuous network. And the CuO NWs can be reduced into highly conductive Cu cores in a low temperature H_2 annealing. In this way, we have demonstrated an excellent cycling stability that last more than 700 (or 1000) charge/discharge cycles at a current density of 3.6A/g (or 1A/g), with a high capacity retention rate of 80%. Remarkably, these Cu/a-Si core-shell anode structure can survive extremely high charging current density of 64A/g for 25 runs, and then recover 75% initial capacity when returning to 1A/g. We also present the first and straigthforward experimental proof that these robust highly-cross-linked core-shell network can preserve the structural integrity even after 1000 runs of cycling. All hese results indicate a new and convenient strategy towards a high performance Si-loaded battery application.

Introduction

The ever-increasing demand for high performance lithium ion batteries (LIBs), catering to the needs of emerging portable electronic devices, medical devices and electric/hybrid electric vehicles, has spurred world-wide research efforts to explore alternative high capacity anode materials [1-3], which include silicon (Si), germanium (Ge), tin (Sn), SnO_2 and several transition metal oxides[4]. Among them, Si boasts the highest known specific capacity with a maximum theoretical value of 4200 mAh/g (corresponding to a compound state of $Li_{22}Si_5$), which is even higher than that of metallic Li itself (~3800 mAh/g) and thus holds a great promise to serve as high capacity anode materials. However, there remains still a formidable challenge due to the large volume changes of Si anode during lithiation reactions, which amounts to ~400% volume expansion during Li^+ ion insertion, and thus causing permanent pulverization, electrode rupture and very short cycle lifetime. To address these issues and achieve a long term cycling stability of Si-loaded anodes, various nanostructured electrodes, in a form of thin films [5], nano particles (NPs) [6-8] and nanowires (NWs)[9-12] as well as other porous alloys and composites [13-18] have been widely explored. Furthermore, adopting a composite core-shell or hierarchical nanowire-branch structure[19-27] are emerging as a favourable 3D composite architecture, where a thin Si-coating layer allows for a shorter diffusion distance for Li ions and thus an improved rate performance. Compared to crystalline silicon (c-Si), amorphous silicon (a-Si) has a better cycling performance because the volume expansion within a-Si medium is homogeneous and thus has a less chance of pulverization[28]. Exploiting a slightly higher lithiation potential of a-Si (@220 mV) than that of c-Si (@120 mV), Cui Yi's group has demonstrated a c-Si/a-Si core-shell nanowire anode structure, which has a high charge storage capacity ~1000 mAh/g at 0.2C with ~90% capacity retention over 100 cycles[29] ; Recently, Feifei Cao and co-workers demonstrated a CuNW-Si-Al_2O_3 nano-

[a] National Laboratory of Solid State Microstructures and School of Electronics Science and Engineering/Collaborative Innovation Centre of Advanced Microstructures, Nanjing University, Nanjing 210093, China.
Corresponding Emails: yulinwei@nju.edu.cn, wangjz@nju.edu.cn.

† Footnotes relating to the title and/or authors should appear here.
Electronic Supplementary Information (ESI) available: [details of any supplementary information available should be included here]. See

cable array anchored upon a Cu foil as anode collector, with a high capacity of 1560 mAh/g at a charging current density of 1.4 A/g for 100 cycles, or a capability of 790 mAh/g at a large current density of 14 A/g for 5 cycles[30].

Recently, interconnected nanostructures have been proven beneficial in improving the mechanical stability and cycling performance of LIBs. For example, Hung T. Nguyen *et al.* fabricated highly interconnected silicon nanowires (SiNWs) that provide redundant/or backup pathways for the SiNWs that happen to detach from the substrate during charging cycles. In this way, a ~100% charge retention after 40 cycles at C/2 rate has been reported, with a high charge rate up to 8C for several cycles[31]. Yan Yao and co-worker elaborated a novel interconnected Si hollow nano-sphere electrode, which allows large volume changes without pulverization and thus exhibits a high initial capacity of 2725 mAh/g at 0.7A/g, but with still a 8% capacity degradation every hundred cycles [32].

In this work, we propose and demonstrate a highly cross-linked (HCL) Cu/a-Si core-shell anode structure grown upon copper foam substrates as current collector. In such a 3D interconnected core-shell network, the highly conductive Cu cores allows for an effective electron transport, while the a-Si thin film coating serves as both a durable high capacity storage medium and a continuous binding layer join CuO (later reduced to Cu by H_2 annealing) NWs at the crossing points. This highly interconnected geometric feature provides redundant conductive pathways down to the current collector, as well firmly mechanical support and connections against root-rupturing and detachment of individual core-shell nanowires, which are critical capabilities to ensure a long term cycling stability and high rate performance. Assembled as anode materials in a half LIBs, the Cu/a-Si core-shells have demonstrated a high rate charging at current density of 3.6A/g (or 1A/g) for 700 (or 1000) cycles, with still an excellent capacity retention rate and final capacity of 80% and 748 mAh/g (1026 mAh/g), respectively. Remarkably, these Cu/a-Si core-shell-based LIBs can even survive an extremely high charging current density of 64 A/g for 25 runs, and then recover very well with a 75% retention ratio at 1A/g. Finally, we also present the first and straightforward experimental proof of the robust structural integrity of the HCL core-shell nanowires even after 1000 runs of cycling. All these results indicate a novel and convenient strategy for a durable high capacity Si-loaded lithium battery application.

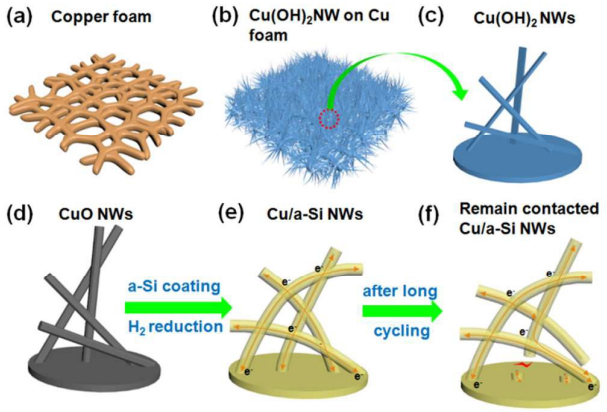

Fig. 1 Schematic diagrams showing the fabrication process of the Cu/a-Si core-shell structures, which includes: (a) Copper foam (b) $Cu(OH)_2$ NWs on Cu foam (c) Amplification of the circle area of (b), cross $Cu(OH)_2$ NWs structure (d) Cross CuO NWs after calcination (e) the highly cross-linked Cu/a-Si core-shell structure; (f) depicts the situation that the broken core-shell nanowires in a highly cross-linked configuration enjoy redundant connection pathways, and thus ensure a durable long cycling performance.

Experiments

(1) Synthesis and Fabrication

The fabrication procedure of the Cu/a-Si core-shell nanowire anode structure has been illustrated schematically in **Fig. 1**: first, a high density matrix of mutual crossing $Cu(OH)_2$ NWs were grown upon a copper foam (5cm*5 cm) by a simple chemical synthesis method in an aqueous solution of 2.5mol/L NaOH and 0.1mol /L $(NH_4)_2S_2O_8$ at room temperature for about 60 min, as depicted in Fig. 1(a)-1(c); Then, the foam was dried with nitrogen and annealed at 350 ^oC in argon ambience for 2 hours to dehydrate $Cu(OH)_2$ NWs into CuO NWs (Fig. 1(d)); In the next step, an a-Si thin layer was deposited over the CuO NWs in a plasma enhanced chemical vapour deposition (PECVD) system by 5 sccm pure SiH_4 for 30 min at 200 ^oC, with a chamber pressure and RF power density of 600 mTorr and 76 mW/cm^2, respectively. The areal Si-loading density over the CuO NWs matrix has been determined to be about 0.18~ 0.21 mg/cm^2; Finally, the sample was annealed at 300 ^oC in H_2 ambient in the PECVD chamber for 240 min to reduce the CuO cores into Cu,

and thus a Cu/a-Si core-shell structure (Fig. 1(e)), with a H_2 flow rate and chamber pressure of 45 SCCM and 600 mTorr, respectively.

(2) Characterizations and Electrochemical measurements

The morphology, structure and chemical composition of the Cu/a-Si core-shell anode structure were characterized by field emission scanning electron microscopy (FE-SEM, Sigma Zeiss), Transmission electron microscopy (TEM, Tecnai G2 F20) and energy dispersive X-ray spectroscopy (EDX, Tecnai G2 F20). The electrochemical properties of the samples were measured in CR2032 coin-type cells assembled in an argon-filled glove box. The cells were formed using a Li metal negative electrode, an electrolyte of 1 M LiPF6 in a 1:1 ethylene carbonate and diethyl carbonate mixture. A galvanostatic cycling test of the assembled cells was carried out on a Land system (BT 2013A). Cyclic voltammetry (CV) characterizations were conducted with an electrochemical workstation (CHI660D) with a two-electrode system incorporating the Cu/a-Si core-shell structure as the working electrode with Li foil as the reference and counter electrodes. The mass load of a-Si was evaluated by a high quality precision electronic balance (Sartorius, BT125D, 0.1 mg).

Results and discussion

The SEM images of the Cu foam substrate, the as-grown $Cu(OH)_2$ NWs, the CuO NWs and the Cu/a-Si core-shell are shown in **Figs. 2**(a)-2(e), respectively. As we can see in Fig. 2(b), with an enlarged view provided in 2(c), the random $Cu(OH)_2$ NWs grown over the rough Cu foam substrate are naturally mutual crossing, with a length of about 20 to 30 um and a diameter ranging from 30 to 60 nm. After calcination at 350 ^{o}C for 2h, the dehydrated CuO NWs are found to become more flexible with slightly bending morphology, as seen in Fig. 2(d). With a subsequent a-Si layer coating, the diameter of the Cu/a-Si core-shell increases to about 200 nm, as witnessed in Fig. 2(e) and 2(f), from which the sidewall-coated a-Si layer is estimated to be ~80 nm thick. More interestingly, a close scrutiny of Fig. 2(f) reveals that the a-Si coating by a plasma enhanced deposition has been quite uniform, which has been able to merge the crossing CuO NWs into a continuous and cross-linked 3D network. This is indeed a desirable feature for building a robust framework for LIB applications.

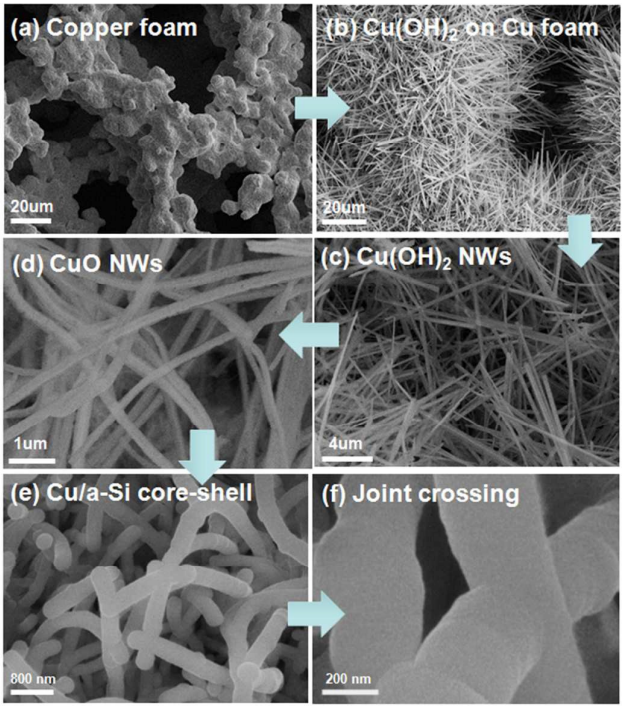

Fig. 2 (a), (b) show the SEM images of the copper foam substrate and the as-grown $Cu(OH)_2$ NWs, with an enlarged view presented in (c); (d) the crossing CuO NWs after calcination; (e) the highly cross-linked Cu/a-Si core-shell nanowires after H_2 reduction at 300 ^{o}C for 4h, while (f) provides a close view of the joint crossing between two nanowires bound by the conformal coating of a-Si layer in PECVD.

Transmission electron microscopy (TEM) characterizations provide more structural details and compositional information of the CuO NWs and the Cu/a-Si core-shell structures. Fig. 3(a) shows a bright-field TEM image of the CuO NWs, while Fig. 3(b) provides a high-resolution TEM lattice view, where a d-spacing of 0.25 nm corresponds to the spacing between CuO (-111) planes [33]. A composition mapping analysis of the CuO NW has been carried out by energy dispersive X-ray (EDX) spectroscopy and presented in Fig. (c), which confirms a complete transformation of the $Cu(OH)_2$ NWs into CuO NWs after the calcination annealing step. Further on, in Fig. 3(d), we show a low-magnification TEM image of an individual Cu/a-Si core-shell nanowire after H_2 reduction treatment. Note that, the a-Si layer here has been intentionally reduced to only 20~30 nm in order to facilitate TEM characterization. Remarkably, the CuO core has been entirely reduced by a simple H_2 annealing into Cu, as inferred from the high-resolution TEM image in Fig. 3(e) exhibiting a d-spacing of 0.21 nm which corresponds to the (111) plane spacing

of Cu lattice[30]. Meanwhile, it is also interesting to note that, though the contrast of the core-shell interface remains still sharp, there seems to be a somewhat Cu migration along the interface that causes a roughening of the Cu/a-Si interface. Nevertheless, the continuity of the Cu core has been preserved, as an important basis for an efficient synergistic core-shell structure.

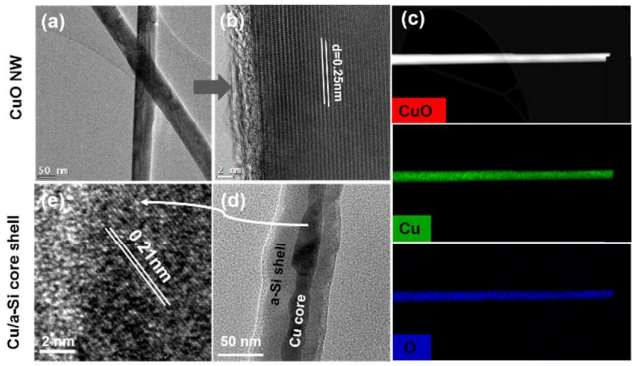

Fig. 3 (a) The Low-resolution and (b) the High-resolution TEM image of the CuO NWs, in which the d-space 0.25 nm indicates the (-111) crystalline plane of CuO. (c) Bright-field TEM image and EDX mapping of Cu and O element in single CuO nanowire. (d) The Low-resolution and (e) the High-resolution TEM image of the Cu/a-Si core-shell NWs, where we can see clearly the a-Si shell and Cu core with the corresponding d-space 0.21 nm implying the (111) crystalline plane of Cu.

According to the XRD analysis of the initial CuO/a-Si and the reduced Cu/a-Si core-shell samples in Fig. 4, the diffraction peaks of CuO all disappear after a simple low temperature H_2 annealing at 300 ^{o}C for 4 hours, indicating a complete transformation of the CuO cores into elemental Cu (as learnt from the emerging of a series of sharp diffraction peaks of Cu lattice). In addition, a trace signal of Cu_3Si(PDF#51-0916) alloy diffraction peaks are also observed at 44.5° and 44.9°, corresponding to the crystalline planes of Cu_3Si (012) and (300), which could result from the mixture and alloying between Si and Cu at the core-shell interface.

To test the electrochemical performance, the highly cross-linked Cu/a-Si core-shell structure was assembled into a LIB half-cell, and tested for their cyclic voltammetry (CV) curves are presented in Fig. 5(a). As we can see, for the first three cycles with a voltage ranging from 0.01 V to 1.1 V at a scan rate of 0.1 mV/s, the Cu/a-Si core-shell NW-based LIB demonstrates a cathodic peak at ~0.18V in the 1st cycle, corresponding to the initial lithiation of a-Si to form a-Li_xSi, which is then followed by a sharp reductive peak at 0.03V assigned to the formation of the crystalline $Li_{15}Si_4$ alloy [34, 35]. During the first charging process, two anodic sharp peaks appear at 0.32V and 0.49 V which can be ascribed to first the phase transition from $Li_{15}Si_4$ alloy back to amorphous Li_xSi, and then the release of Li from Si anode. In the subsequent cycles, the CV curves almost overlap with only a slight shift that may be assigned to the surface change during lithiation cycles[31]. This indicates a good reproducibility and a high reversibility of the redox reaction.

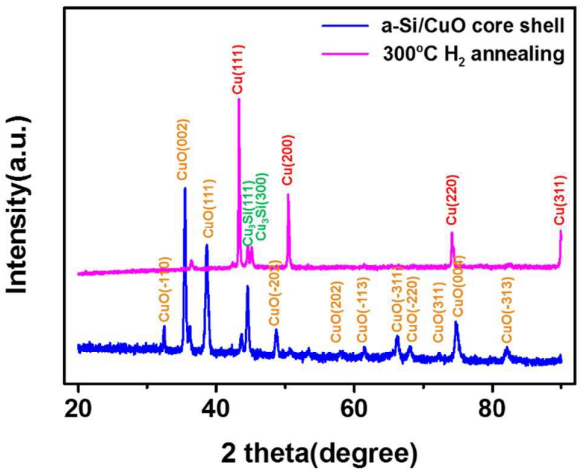

Fig. 4 XRD analysis of Cu/a-SiO core-shell NWs and Cu/a-Si core-shell reduced in H_2 ambient at 300 ^{o}C for 4h, respectively.

Meanwhile, the first five cycles of discharge and charge voltage profiles of Cu/a-Si core-shell based LIB, under a current density of 1.8 A/g, are also shown in Fig. 5(b). The plateaus at ~0.20 V and ~0.05 V during discharge and the plateaus at ~0.30 and ~0.51 during charging are basically consistent to the peaks observed at cyclic voltammetry curves in Fig. 5(a). The small plateaus appearing only in the first cycle, at ~1.70 V and ~1.26V, can be attributed to the presence of CuO remnant in the anode structure during LIB assembling and loading, which could also react with lithium to produce Cu and Li_2O irreversibly under the following voltage window[36]. According to Fig. 5(c), after the 5 initial cycles to stabilize the SEI layer and activate the storage medium (with a relatively low current density of 0.5 A/g), the highly cross-linked (HCL) Cu/a-Si core-shell anode exhibits a specific capacity of 1730m Ah/g, with a retention rate of 81% after 150 cycles at a current density of 2 A/g, which compares favourably over the non-cross-linked (NCL) Cu/a-Si core-shell reference, where the CuO NWs were fabricated with a

thermal oxidation of flat copper plate that leads to a matrix of separated CuO NWs with little mutual-crossing, as witnessed in the Supplementary Material S. 1. The latter one, with little cross-linking, demonstrates a similar capacity but with only a retention rate of 61% after 150 cycles. This highlights the benefit of a highly cross-linked Cu/a-Si core-shell structure, which has played an important role to enhance anode electrode's cycling stability.

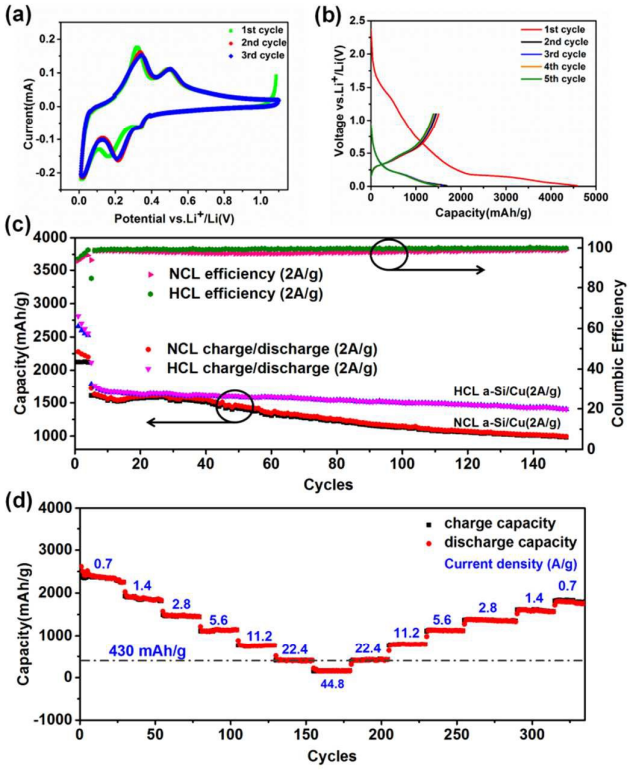

Fig. 5 Li-ion battery cycling performance of highly cross-linked (HCL) Cu/a-Si anode materials between 0.01 V and 1.1 V: (a) cyclic voltammetry curves for the first three cycles of Cu/a-Si core-shell anode at the scan rate of 0.0001 V/s with the voltage rang of 0.01 V-1.1 V, (b) voltage profiles of the first five cycles at 1.8 A/g (c) the discharge capacities and corresponding Columbic efficiencies of highly cross-linked (HCL) Cu/a-Si anode with the discharge/charge current of 2.0 A/g over 150 cycles, and non-cross-linked (NCL) Cu/a-Si core-shell anode at a current density of 2.0 A/g, respectively and (d) show rate capability from 0.7 A/g to 44.8 A/g discharge/charge current.

The rate capability of the 3D highly cross-linked core-shell structure has been tested and shown in Fig. 5(d). We found that the Cu/a-Si core-shell structure can reach a high specific capacity of 2616 mAh/g at a current density of 0.7 A/g. With the increase of the charging current density from 1.4 A/g to 2.8 A/g, 5.6 A/g, 11.2A/g and 22.4 A/g, the reversible capacity decreases gradually from 1936 mAh/g, to 1485 mAh/g, 1109 mAh/g, 770m Ah/g and 430 mAh/g, respectively. Even at an extremely fast current density of 44.8 A/g (corresponding to 150 s for a full charge and discharge), the electrode could deliver a stable capacity of above 200 mAh/g. More importantly, when the charging current density is reset to 0.7A/g by step, a series of capacity retention rates of 104%, 103%, 100%, 93%, 87% and 80% are recorded for current densities at 22.4 A/g, 11.2 A/g, 5.6 A/g 2.8 A/g, 1.4 A/g and 0.7 A/g. These results demonstrate a superior high rate performance of the 3D highly cross-linked Cu/a-Si core-shell structure. According to the electrochemical impedance spectra (EIS) of the core-shell LIBs, during the first 6 runs of cycling, shown in the Supplementary Material S.2, the extracted impedances start at around 24 Ohm, and then stabilize at 15 Ohm, indicating the Cu NW cores are indeed highly conductive, thus accounting for a major reason for achieving such an excellent high rate performance of the Cu/a-Si core-shell nanowire-based LIBs.

Furthermore, the Cu/a-Si core-shell anodes feature also an excellent long-term cycling performance thanks to a firmly anchoring to the copper foam and a redundant connection pathway enjoyed by a highly cross-linked network. Fig. 6(a) shows the discharge/charge capacity evolution of the Cu/a-Si core-shell electrode at current density 3.6 A/g up to 700 cycles. A rising of capacity can be seen during the starting cycles due to the activation process of the amorphous Si medium. A final capacity of 748 mAh/g could be obtained with an 80% retention rate with a Columbic efficiency > 97%.

More importantly, in a combined testing of the high rate capability and long term cycling stability performance, the Cu/a-Si core-shell structure anodes experienced firstly a series of high rate charging and discharging operations, with a charge current density ramping from 0.5A/g to 64A/g for 25 cycles at each rate step as seen in Fig. 6(b), which is then followed by a continuous cycling at 1 A/g until 1000 runs. As we can see, a reasonably high 80% retention rate has been recorded with a final capacity of 1026 mAh/g at the end of 1000 cycles, indicating that the highly cross-linked Cu/a-Si

core-shell structure is indeed quite stable and robust against both the high rate and long term cycling operations.

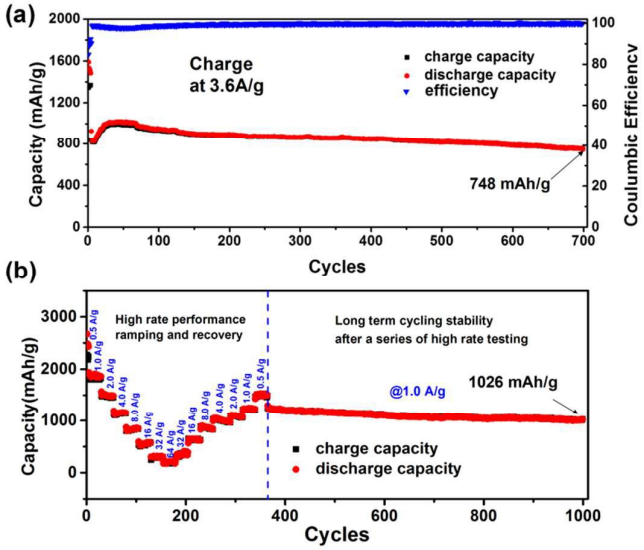

Fig. 6 Li-ion battery cycling performance of Cu/a-Si anode materials between 0.01 V and 1.1 V: (a) Long-term cycle performance of highly cross-linked Cu/a-Si core-shell anode (b) Rate performance and following long term cycling at a current of 1 A/g.

For example, compared to a similar a-Si loaded Cu NWs anode structure in Ref. [30], where the Cu/a-Si NWs core-shell structure are fabricated upon flat copper plate and thus with little crossing, the highly cross-linked core-shell structure reported here exhibits an excellent cycling stability (lasting up to 1000 runs, compared to that of below 100 runs with a similar charge current density). Actually, achieving simultaneously a high rate performance and a long term cycling stability of the interconnected Cu/a-Si core-shell anode electrode can be attributed to the fact that, the cross-linked Cu/a-Si core-shell NWs provide a high number of redundant or backup conductive pathways, thanks to the conformal coating and binding of a-Si layer coating layer deposited in a PECVD system. This is particularly important for long term cycling stability, as the nanowire-based anode structures are all vulnerable to root-rupturing or breakage during the cycling. Once this happens, individual core-shell units will lose contact immediately with the current collector and detach from the substrate, causing permanent and rapid capacity deterioration. In strong contrast, as illustrated in Figs. 1(e) and 1(f), within a highly cross-linked network, a broken core-shell unit has still a chance to be held by neighbouring cross-linked NWs, and thus preserves the electric connection and remains as still active storage medium. This geometric advantage, together with a synergetic core-shell structure with a very conductive Cu core, has been the key to establish a really robust, accommodative and durable 3D network of Si-loaded LIB applications.

A straightforward examination of this benefit has been provided in Fig. 7, where the SEM images of the core-shell anode structures, after long term cycling, with highly-cross-linked or non-cross-linked features are presented and compared. Strikingly, as we can see in Figs. 7(a) and 7(b), after 1000 runs of cycling, the highly-cross-linked anode structure develops relatively much thinner cracking, among which highly interconnected and continuous core-shell nanowires are still well preserved. This observation provides the first experimental proof of the robust structural property of the highly cross-linked Cu/a-Si core-shell nanowires, after long term cycling operations. In strong contrast, for the non-cross-linked ones, huge cracks (note that, the scale bar in Fig. 7(c) is 40 um, much larger than that in Fig. 7(a) for HCL) are found that leading to easy peeling off from the substrate, while the initially less-crossing core-shell structures all merge into a thick single piece layer with little flexibility to guarantee the integrity of the anode structure. This also explains why a poor cycling performance has been achieved for the LIBs of this kind.

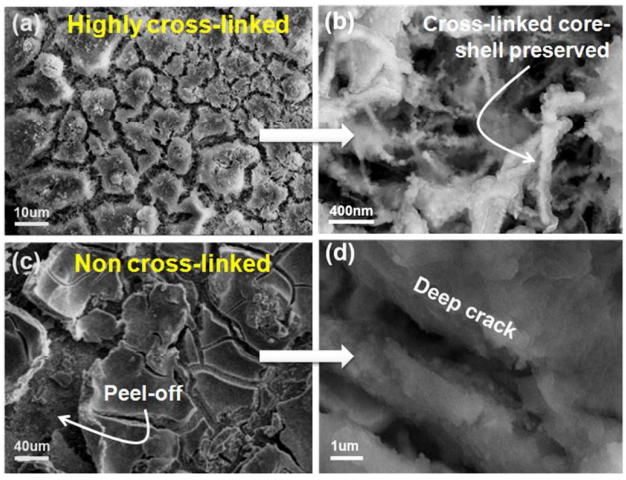

Fig. 7 SEM images of the core-shell nanowire structure with (a) or without (c) a highly cross-linked geometric feature, with their corresponding enlarged views of the network and crack details shown in (b) and (d), respectively.

Finally, we also extract the battery performance of the Cu/a-Si core-shell nanowire anode structure, and compare them to the Si-loaded and mostly nanowire-based LIBs in the literature, as summarized in Table 1 in Supplementary Materials. As we can see, the highly cross-linked core-shell structure has demonstrated indeed an outstanding long term cycling stability (lasting more than 1000 cycles), with a very high rate performance and retention ration. All these results indicate that this simple and efficient Cu/a-Si core-shell structures could represent a new strategy to fulfil the potential of Si-loaded lithium ions battery applications.

Conclusions

In summary, we have proposed and demonstrated a new 3D cross-linked Cu/a-Si core-shell structure, fabricated directly from copper foam as current collector substrate, which has enabled high capacity, high rate and durable Si-loaded LIBs with a high specific capacity ~928 mA/g (80% capacity retain) after 700 charge and discharge cycles at a high current density of 3.6 A/g. Furthermore, even after an extremely high rate performance testing under a current density up to 64 A/g, this highly interconnected Cu/a-Si core-shell structure anode can hold a capacity retention rate of 80% (a final capacity of 1026mAh/g) up to 1000 cycles at a 1A/g current density. We suggest that this cross-linked structure could also indicate a promising new route towards a new generation of high capacity Si-loaded Li-ion batteries.

Acknowledgements

This work is partly supported by Jiangsu Province Natural Science Foundation (Young Talent Program No. BK20130573) , Jiangsu province (BRA 2015284) and National Basic Research 973 Program under Grants 2014CB921101, 2013CB932900, 2013CB632101, 2010CB934402 and NSFC under Nos. 11274155 and 61204050, and the Fundamental Research Funds for the Central Universities.

Notes and references

1 B. Kang and G. Ceder, Nature, 2009, 458, 190-193.
2 M. Armand and J.-M. Tarascon, Nature, 2008, 451, 652-657.
3 D. Larcher and J. M. Tarascon, Nat. Chem., 2015, 7, 19-29.
4 P. Roy and S. K. Srivastava, J. Mater. Chem. A, 2015, 3, 2454-2484.
5 W. P. Si, X. L. Sun, X. H. Liu, L. X. Xi, Y. D. Jia, C. L. Yan and O. G. Schmidt, J. Power Sources, 2014, 267, 629-634.
6 X. L. Wang, G. Li, F. M. Hassan, M. Li, K. Feng, X. C. Xiao and Z. W. Chen, J. Mater. Chem. A, 2015, 3, 3962-3967.
7 N. Liu, Z. D. Lu, J. Zhao, M. T. McDowell, H. W. Lee, W. T. Zhao and Y. Cui, Nat. Nanotechnol., 2014, 9, 187-192.
8 S. Fang, L. F. Shen, Z. K. Tong, H. Zheng, F. Zhang and X. G. Zhang, Nanoscale, 2015, 7, 7409-7414.
9 L.-F. Cui, Y. Yang, C.-M. Hsu and Y. Cui, Nano Lett., 2009, 9, 3370-3374.
10 C. K. Chan, H. Peng, G. Liu, K. McIlwrath, X. F. Zhang, R. A. Huggins and Y. Cui, Nat. Nanotechnol., 2008, 3, 31-35.
11 H. Wu, G. Chan, J. W. Choi, I. Ryu, Y. Yao, M. T. McDowell, S. W. Lee, A. Jackson, Y. Yang, L. Hu and Y. Cui, Nat. Nanotechnol., 2012, 7, 310-315.
12 S. J. Jing, H. Jiang, Y. J. Hu and C. Z. Li, Nanoscale, 2014, 6, 14441-14445.
13 G. Kim, S. Jeong, J.-H. Shin, J. Cho and H. Lee, ACS Nano, 2014, 8, 1907-1912.
14 S. A. Klankowski, G. P. Pandey, B. A. Cruden, J. W. Liu, J. Wu, R. A. Rojeski and J. Li, J. Power Sources, 2015, 276, 73-79.
15 J. Y. Liu, N. Li, M. D. Goodman, H. G. Zhang, E. S. Epstein, B. Huang, Z. Pan, J. Kim, J. H. Choi and X. J. Huang, ACS Nano, 2015, 9, 1985-1994.
16 X. J. Feng, J. Yang, Y. T. Bie, J. L. Wang, Y. Nuli and W. Lu, Nanoscale, 2014, 6, 12532-12539.
17 Y. X. Tang, Y. Y. Zhang, J. Y. Deng, D. P. Qi, W. R. Leow, J. Q. Wei, S. Y. Yin, Z. L. Dong, R. Yazami, Z. Chen and X. D. Chen, Angew. Chem. Int. Ed. Engl., 2014, 53, 13488-13492.
18 Y. X. Tang, Y. Y. Zhang, J. Y. Deng, J. Q. Wei, H. Le Tam, B. K. Chandran, Z. L. Dong, Z. Chen and X. D. Chen, Adv. Mater., 2014, 26, 6111-6118.
19 H. Wu and Y. Cui, Nano Today, 2012, 7, 414-429.
20 Y. X. Tang, Y. Y. Zhang, W. L. Li, B. Ma and X. D. Chen, Chem. Soc. Rev., 2015, 44, 5926-5940.
21 J. Xie, X. G. Yang, S. Zhou and D. W. Wang, ACS Nano, 2011, 5, 9225-9231.
22 X. L. Chen, K. Gerasopoulos, J. C. Guo, A. Brown, C. S. Wang, R. Ghodssi and J. N. Culver, ACS Nano, 2010, 4, 5366-5372.
23 H. T. Nguyen, M. R. Zamfir, L. D. Duong, Y. H. Lee, P. Bondavalli and D. Pribat, J. Mater. Chem., 2012, 22, 24618.
24 K. Kang, K. Song, H. Heo, S. Yoo, G.-S. Kim, G. Lee, Y.-M. Kang and M.-H. Jo, Chem.Sci., 2011, 2, 1090.
25 H. J. Lin, W. Weng, J. Ren, L. B. Qiu, Z. T. Zhang, P. N. Chen, X. L. Chen, J. Deng, Y. G. Wang and H. S. Peng, Adv. Mater., 2014, 26, 1217-1222.
26 Y. Fan, Q. Zhang, Q. Z. Xiao, X. H. Wang and K. Huang, Carbon, 2013, 59, 264-269.
27 Y. Fan, Q. Zhang, C. X. Lu, Q. Z. Xiao, X. H. Wang and B. K. Tay, Nanoscale, 2013, 5, 1503-1506.
28 M. T. McDowell, S. W. Lee, W. D. Nix and Y. Cui, Adv. Mater., 2013, 25, 4966-4985.
29 L.-F. Cui, R. Ruffo, C. K. Chan, H. L. Peng and Y. Cui, Nano Lett., 2008, 9, 491-495.
30 F. F. Cao, J. W. Deng, S. Xin, H. X. Ji, O. G. Schmidt, L. J. Wan and Y. G. Guo, Adv. Mater., 2011, 23, 4415-4420.
31 H. T. Nguyen, F. Yao, M. R. Zamfir, C. Biswas, K. P. So, Y. H. Lee, S. M. Kim, S. N. Cha, J. M. Kim and D. Pribat, Adv. Energy Mater., 2011, 1, 1154-1161.

32 Y. Yao, M. T. McDowell, I. Ryu, H. Wu, N. Liu, L. B. Hu, W. D. Nix and Y. Cui, Nano Lett., 2011, 11, 2949-2954.
33 J. Wang, Q. B. Zhang, X. H. Li, B. Zhang, L. Q. Mai and K. L. Zhang, Nano Energy, 2015, 12, 437-446.
34 N. Wang, T. Hang, H. Q. Ling, A. Hu and M. Li, J. Mater. Chem. A, 2015, 3, 11912-11919.
35 H. Wu, N. Du, H. Zhang and D. Yang, J. Mater. Chem. A, 2014, 2, 20510-20514.
36 A. Débart, L. Dupont, P. Poizot, J. B. Leriche and J. M. Tarascon, J. Electrochem. Soc., 2001, 148, A1266.